Proc. of International Conference on Artificial Intelligence, Computer, Data Sciences and Applications (ACDSA 2025)
7-9 August 2025, Antalya-Türkiye

Numerical simulations of non-fluorescent states of carboxyfluoresceins in presence of heavy iodine ions

Selim Can Dirican
Mechanical Engineering
Özyeğin University
Istanbul, Türkiye
can.dirican@ozu.edu.tr

Süleyman Yiğit Dölek
Electrical and Electronics Engineering
Özyeğin University
Istanbul, Türkiye
yigit.dolek@ozu.edu.tr

Bahar Tezcan
Computer Science
Özyeğin University
Istanbul, Türkiye
bahar.tezcan@ozu.edu.tr

Eren Kaan Demirlek
Computer Science
Özyeğin University
Istanbul, Türkiye
kaan.demirlek@ozu.edu.tr

Yavuz Alparslan Yılmaz
Computer Science
Özyeğin University
Istanbul, Türkiye
alparslan.yilmaz@ozu.edu.tr

Barış Demirbay
Mathematical and Natural Sciences
Özyeğin University
Istanbul, Türkiye
baris.demirbay@ozyegin.edu.tr

***Abstract*—In the present research, the effects of heavy iodine ions on dark transient state populations of carboxyfluorescein derivatives, each with a different number of bromine atoms attached, were computationally examined via numerical simulations adapted to a widefield fluorescence microscopy integrated with a microfluidics platform. Numerical simulations were carried out by considering geometrical profile of excitation laser beam, microscopy and microfluidics parameters of a proposed experimental design as well as electronic transition rates of fluorescent molecules. Electronic state model of studied dyes was treated as a system of first order ordinary differential equations and time-dependent solutions of long-lived, non-fluorescent dark state populations were computed for each dye at varying potassium-iodine [KI] concentrations. Analytical solutions of state populations were then adapted to a proposed experimental setup to systematically analyze how dark state populations evolve when carboxyfluorescein derivatives pass through excitation beam field in a microfluidics chip under different flow speeds. Computational experiments have successfully uncovered systematic changes in dark triplet and photo-oxidized state populations upon the addition of iodine ions into fluorophore solutions.**

Keywords*—Photophysics, external heavy atom effect, fluorophores, fluorescence microscopy, microfluidics, numerical simulations

I. Introduction

The presence of heavy atoms in the same environment as fluorescent molecules (fluorophores) significantly influences their photophysical behavior, particularly by enhancing intersystem crossing (ISC) rates through spin-orbit coupling [1]. This effect is commonly referred to as the heavy atom effect and can be categorized into two categories, which are internal and external heavy atom effects [2]. While the internal heavy atom effect arises from covalently bound heavy elements within a fluorophore's molecular structure, the external heavy atom effect is induced by the incorporation of heavy ions into the surrounding medium. The latter provides a versatile approach to modulate the ISC process without chemically modifying the fluorophore [3]. External heavy atoms, such as iodine, interact with photo-excited fluorophores via spin-orbit coupling, facilitating non-radiative transitions from the singlet excited state to the triplet state or even longer-lived radical states. These transitions lead to an increase in the population of dark transient states, which are particularly useful in fluorescence-based applications such as imaging [4], biosensing [5], and photodynamic therapy [6]. By carefully modulating the concentration of external heavy atoms, ISC rates and triplet state lifetimes can be fine-tuned to optimize fluorescence signals, reduce photobleaching, and improve photostability of fluorophores under continuous laser excitation.

Leveraging the external heavy atom effect in fluorescence spectroscopy presents additional experimental challenges. ISC rate enhancements caused by heavy ions can lead to complex transient dark-state dynamics, requiring advanced detection methods to resolve them accurately. Conventional single-molecule detection (SMD) methods, often struggle with insufficient photon statistics, fluorescence saturation, and inconsistent excitation profiles, which hinder precise characterization of these transitions [7]. Additionally, the uneven distribution of excitation intensity in confocal and point-scanning microscopy methods further complicates the analysis of dark transient states. To tackle these challenges, this research

The authors gratefully acknowledge financial support (a grant number 124F110) provided by The Scientific and Technological Research Council of Türkiye (TÜBİTAK).

979-8-3315-3562-9/25/$31.00 ©2025 IEEE

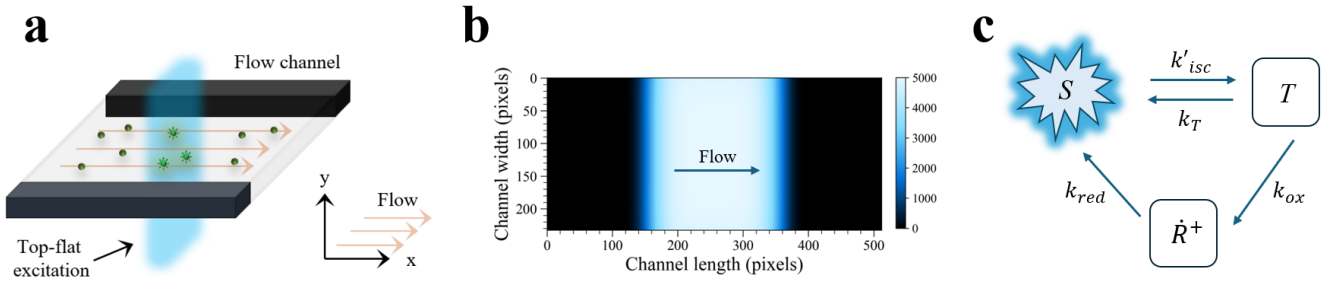

Fig. 1. (a) A schematic of microfluidics platform, (b) simulated flat-top laser beam profile and (c) electronic state model of CFl-based fluorophores with transition rates where S, T and $\dot{R}^+$ denote fluorescent singlet, triplet and photo-oxidized states, respectively.

presents a novel numerical simulation method for monitoring the impact of external heavy ions on the photophysical transitions of carboxyfluorescein (CFl) and its brominated derivatives, which are mono-bromo-carboxyfluorescein (CFl-1Br), di-bromo-carboxyfluorescein (CFl-2Br) and tetra-bromo-carboxyfluorescein (CFl-4Br), respectively. With proposed numerical simulations adapted to a microfluidic-based widefield fluorescence microscopy, we explore how varying potassium iodide [KI] concentrations, and flow rates influence non-fluorescent triplet (T) and photo-oxidized state ($\dot{R}^+$) populations of these dyes. By employing a flat-top excitation profile, our method ensures uniform excitation conditions, significantly reducing the risk of photobleaching and improving the accuracy of fluorescence signal measurements [8]. Computational results can provide useful insights into optimizing fluorescence-based detection techniques and contribute to the development of more robust methodologies for studying dark transient states of complex fluorophores in live cells.

II. Methodology

Computational experiments were carried out in Anaconda Navigator (Python) through using numpy, matplotlib and scipy libraries. Details regarding computational data, numerical simulations and analytical treatment of electronic state (photophysical) model were provided in sections A and B.

A. Computational data and numerical simulations

Numerical simulations based on the electronic state model were adapted for integration with a wide-field fluorescence microscopy system coupled to a microfluidic platform, as illustrated in Fig. 1(a). This setup allows precise control over the dark state populations of CFl and its brominated derivatives, which flow over uniform laser excitation beam at a constant laminar flow rate. The output data consists of 2D fluorescence image data, $F(x, y)$, which is numerically simulated using microscopy, laser and electronic transition rate parameters. An example experimental setup, which was previously established to record a series of fluorescence images from flowing fluorescent samples using a high-speed sCMOS camera, can be found from [9] in greater detail. In the present study, camera image of the laser excitation beam profile is first simulated, followed by the fluorescence signal images for each CFl derivative, separately. The fluorescence brightness image of the laser excitation profile (a stretched flat-top laser beam positioned on a microfluidic chip), $I(x, y)$ is computed using a super-Gaussian function [10], as given by the following equation:

$$I(x,y) = I_0 \cdot e^{-2\left(\left(\frac{x-x_0}{w_1}\right)^n + \left(\frac{y-y_0}{w_2}\right)^n\right)} \quad (1)$$

where I_0 is the peak value of fluorescence brightness, w_1 and w_2 are the beam waist radius values of the excitation beams along and across the flow direction, n is the order of beam and this value was fixed to 6, and x and y represent the total number of pixels in the horizontal and vertical dimensions of the image, respectively. x_0 and y_0 denote the peak positions of the laser beam, respectively. The generated images consist of 512 pixels horizontally and 233 pixels vertically. The center coordinates of the laser beams were set to $x_0 = 256$ and $y_0 = 117$ pixels, while w_1, w_2 and I_0 were fixed at 116 pixels, 233 pixels and 5000 a.u., respectively. The simulated laser beam profile was exemplified in Fig. 1(b). Considering a 60× magnification factor of the microscope objective, a 4×4 binning setting of the camera, and a pixel size of 6.5 μm, horizontal and vertical dimensions of image data can be converted to 220.2 μm and 100.2 μm [11]. Other experimental parameters employed in simulations were tabulated in Table I.

TABLE I.
Experimental Parameters used in Numerical Simulations

Parameter	Value / Specification
Excitation Wavelength	488 nm
Beam Profile	Flat-top (super-Gaussian, n = 6)
Beam Waist Radius in x (w_1)	50 μm
Beam Waist Radius in y (w_2)	100.2 μm
Excitation Intensity (I_{exc})	3.62 kW/cm^2
Flow Channel Dimensions	220.2 μm × 100.2 μm × 50 μm
Flow Rates	10 and 2000 μL/min
Microscope Objective	60× water immersion
Pixel Size (sCMOS Camera)	0.43 μm (with 4×4 binning)

The peak value of excitation irradiance (I_{exc}) applied for photo-excitation is directly proportional to effective laser

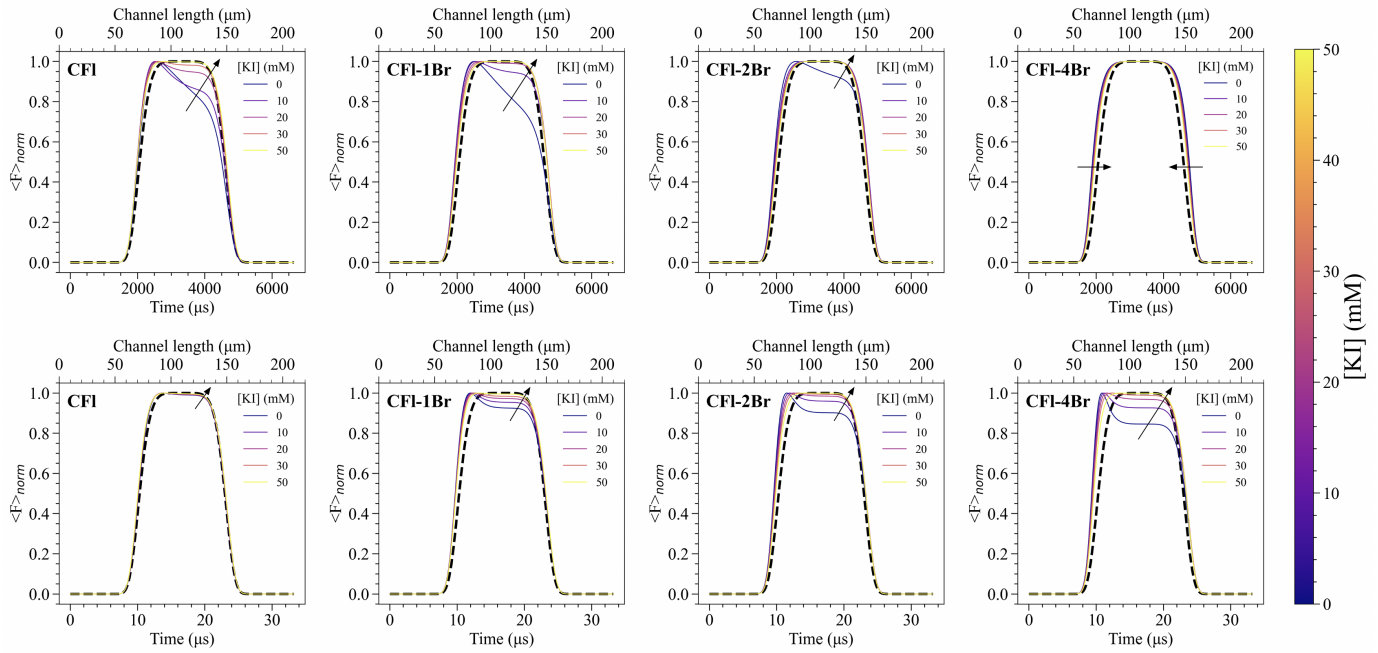

Fig. 2. The effect of [KI] on $< F_{\text{norm}} >$ signals of CFl, CFl-1Br, CFl-2Br and CFl-4Br at 10 μL/min (first row) and 2000 μL/min (second row), respectively. Black dashed line presents laser beam profile without dark states.

power P_{eff} measured at the back aperture of the microscope objective and it can be computed by the following equation:

$$I_{\text{exc}} = \frac{3\sqrt[6]{2}}{\Gamma(1/6)} \frac{P_{\text{eff}}}{w_1 w_2} \tag{2}$$

where $\Gamma(1/6)$ is approximated to 5.57 [12], w_1, w_2 and P_{eff} values were fixed to 50 μm, 100.2 μm and 300 mW to achieve excitation irradiance of 3.62 kW/cm^2.

B. Electronic state modeling of CFl-based fluorophores

Having set the spatial parameters of the image data and the profile of the laser beam, one can simulate the fluorescence and dark state population signals. Using simulated laser beam profile as excitation rate k_{01}, together with the electronic state model proposed for brominated CFls, fluorescence signal images for the specimens can be generated by computing the fluorescent singlet $S(t)$ state in terms of electronic transition rates and photophysical parameters that are tabulated in Table II. Proposed model was presented in Fig. 1(c) and was solved to simulate dark transient states and fluorescence signals of molecules flowing over a uniform flat-top beam area [13]. The model involves singlet (S), triplet (T), and photo-oxidized radical states ($\dot{R}^+$). The population of each state is governed by a set of coupled first-order differential equations as below [14]:

$$\frac{d}{dt}\begin{bmatrix} S(t) \\ T(t) \\ \dot{R}^+(t) \end{bmatrix} = \begin{bmatrix} -k'_{\text{isc}} & k_T & k_{\text{red}} \\ k'_{\text{isc}} & -k_{\text{ox}} - k_T & 0 \\ 0 & k_{\text{ox}} & -k_{\text{red}} \end{bmatrix} \begin{bmatrix} S(t) \\ T(t) \\ \dot{R}^+(t) \end{bmatrix} \tag{3}$$

where k'_{isc} is the effective intersystem crossing rate from excited S state to T, k_T is the triplet relaxation rate, k_{ox} is the oxidation rate from T to $\dot{R}^+$, and k_{red} is the reduction rate from $\dot{R}^+$ to ground state of S. The initial condition assumes that all molecules are in the singlet ground state at $t = 0$, thereby:

$$S(0) = 1, \quad T(0) = 0, \quad \dot{R}^+(0) = 0. \tag{4}$$

The excitation rate from S_0 to S_1 in S state is then given by:

$$k_{01} = \sigma_{\text{exc}} \cdot \frac{I_{\text{exc}}}{E} \tag{5}$$

where σ_{exc} is the excitation cross-section of fluorophore, I_{exc} is the excitation irradiance of laser beam, and E is the energy of incident photons. The effective intersystem crossing rate (k'_{isc}) is defined as:

$$k'_{\text{isc}} = k_{\text{isc}} \cdot \frac{k_{01}}{k_{01} + k_{10}} \tag{6}$$

where k_{isc} is the intrinsic ISC rate, and k_{10} is the radiative decay rate from S_1 to S_0, given by:

$$k_{10} = \frac{1}{\tau_f} - k'_{\text{isc}} - k_{\text{ox}} \tag{7}$$

where τ_f is the fluorescence lifetime of the fluorescent molecule. The singlet state population $S(t)$ over time is obtained by solving the eigenvalue problem of the rate matrix, leading to:

$$S(t) = C_1 e^{\lambda_1 t} + C_2 e^{\lambda_2 t} + C_3 e^{\lambda_3 t}, \tag{8}$$

where $\lambda_1, \lambda_2, \lambda_3$ are the relaxation mode rates and C_1, C_2, C_3 are the amplitudes depending on the electronic transition rates. Detailed solution to S state can be found from ref. [14].

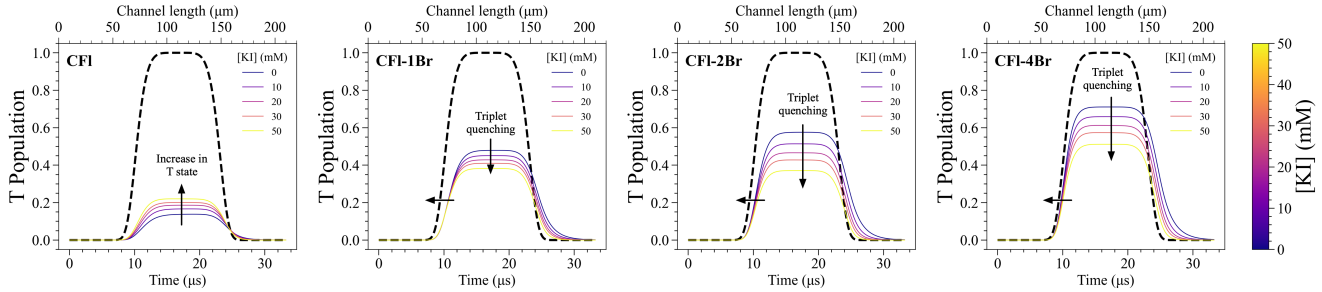

Fig. 3. The effect of [KI] on T state populations of CFl, CFl-1Br, CFl-2Br and CFl-4Br at 2000 μL/min where black dashed line represents the excitation beam profile that has no dark transient states.

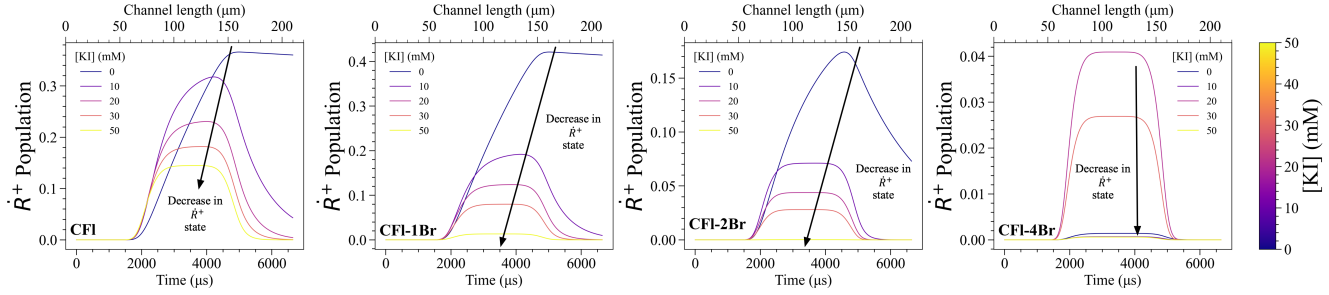

Fig. 4. The effect of [KI] on $\dot{R}^{+}(t)$ state populations of CFl, CFl-1Br, CFl-2Br and CFl-4Br at 10 μL/min.

The duration of laser exposure for flowing molecules can be controlled by modifying the flow speeds within a microfluidic cell. For this reason, considering the pixel information, the fluorescence signals are computed as time-averaged fluorescence signals $< F(t) >$ by using $t = x/v$ where v is the ratio of flow rate to cross-section area (set to 50×100 μm^2) of a flow chip. Combining k_{01} with explicit solution of $S(t)$, the time-averaged fluorescence intensity signal detected from fluorophores is approximated by:

$$\langle F(t)\rangle = k_{10} q_D q_F S(t) \frac{k_{01}(t)}{k_{01}(t) + k_{10}} \tag{9}$$

where q_D is the quantum detection efficiency of the camera, and q_F is the fluorescence quantum yield. For numerical simulations, the fluorescence signal is normalized as:

$$\langle F\rangle_{\text{norm}} = \frac{\langle F(t)\rangle}{\max(\langle F(t)\rangle)} \tag{10}$$

by eliminating experimental dependencies on q_D and q_F. The presence of dark T and $\dot{R}^{+}(t)$ states manifest as fluorescence broadening, shifts or decay behaviors in simulated $< F_{\text{norm}} >$ curves when compared to laser beam profile. In $< F_{\text{norm}} >$ simulations, the flow rates of 10 μL/min and 2000 μL/min were tested and parameters collected from ref. [14] were used to acquire these dark state populations at different time scales. Simulation results were presented in Section III.

III. Computational Results and Discussion

Having performed extensive computational simulations for CFl, CFl-1Br, CFl-2Br and CFl-4Br molecules in our previous study [15], the most optimal excitation irradiance value to investigate the build-up of dark transient states was found to be 3.62 kW/cm^2 by varying flow rates up to 2000 μL/min. Since T and $\dot{R}^{+}$ states can become more pronounced at different flow rates, we first studied the effect of [KI] on $< F_{\text{norm}} >$ signals of each dye at 2 different flow rates, that are 10 μL/min and 2000 μL/min, and the results were presented in Fig. 2. At the flow rate of 10 μL/min, increasing [KI] concentration from 0 to 50 mM leads to a narrowing of $< F_{\text{norm}} >$ signals of each fluorophore inwards the laser beam profile (pointed out by the dashed black line in each subplot). This is clearly seen particularly for CFl-4Br molecule. In the same direction as laminar flow, decays in $< F_{\text{norm}} >$ signals obtained for CFl, CFl-1Br and CFl-2Br become much lower when [KI] concentration is increased from 0 to 50 mM in solvent environment. In the absence of [KI], broadened signals and $< F_{\text{norm}} >$ decays originate from internal heavy atom effects of Br atoms bound to molecular structure of CFl. However, broadening and signal decay effects are not observed upon incorporating heavy I^{-} ions into the solvent, which can be attributed to fluorescence recovery. The same effect was also seen in $< F_{\text{norm}} >$ signals of studied molecules at the highest flow rate of 2000 μL/min. In contrast to $< F_{\text{norm}} >$ signals of CFl-4Br at 10 μL/min flow rate, a strong decay was seen when flow rate is increased to 2000 μL/min in the absence of I^{-} ions. However, systematic addition of [KI] also lowers the decays at faster passage times in microfluidic cell.

In order to examine whether the effects of heavy I^{-} ions on long-lived dark T and $\dot{R}^{+}$ states can be monitored, populations

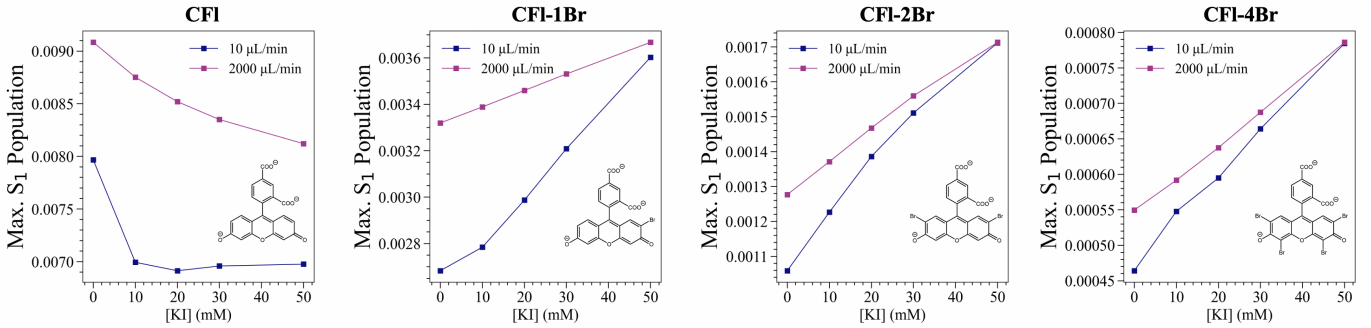

Fig. 5. The effect of [KI] on maximum S_1 state populations of CFl, CFl-1Br, CFl-2Br and CFl-4Br at flow rates of 10 μL/min and 2000 μL/min.

TABLE II.
PHOTOPHYSICAL PARAMETERS AND ELECTRONIC TRANSITION RATES OF CFL DERIVATIVES AT VARIOUS [KI] CONCENTRATIONS.

Fluorophore	τ_F (ns)	σ_{exc} (cm^2)	[KI] (mM)	k_{isc} (μs^{-1})	k_T (μs^{-1})	k_{ox} (μs^{-1})	k_{red} (μs^{-1})
CFl	4.04	3×10^{-16}	0	10.8	0.70	0.00124	0.00001
			10	15.0	0.83	0.00287	0.00101
			20	20.2	0.96	0.00312	0.00201
			30	25.4	1.09	0.00320	0.00301
			50	35.8	1.35	0.00370	0.00501
CFl-1Br	2.71	2.52×10^{-16}	0	94.5	0.605	0.000433	0.0000104
			10	99.69	0.714	0.000821	0.001564
			20	104.88	0.823	0.001000	0.003024
			30	110.07	0.932	0.000960	0.004484
			50	120.45	1.15	0.000266	0.007404
CFl-2Br	1.77	1.77×10^{-16}	0	304.00	0.608	0.000238	0.000472
			10	309.43	0.792	0.000785	0.004292
			20	314.86	0.976	0.000989	0.009112
			30	320.29	1.160	0.001000	0.013932
			50	331.15	1.528	0.000010	0.023572
CFl-4Br	1.12	1.65×10^{-16}	0	893.00	0.584	0.000010	0.0050
			10	895.43	0.745	0.000010	0.00970
			20	897.86	0.906	0.001000	0.01440
			30	900.29	1.067	0.000917	0.01910
			50	905.15	1.289	0.000034	0.02850

of these states were simulated at different flow rates using the same excitation irradiance of 3.62 kW/cm^2. Since transitions from fluorescent S_1 state to T state takes place only within a few μs, T state populations of each dye were carried out at the highest flow rate of 2000 μL/min to achieve this fast time scale. Computational results were plotted in Fig. 3. As can be seen, I^- ions have been found to act differently when they are incorporated into the solvents of bromine containing CFls. It is known that the addition of [KI] can have contrasting effects on different fluorophores. [KI] enhances T state formation in xanthene fluorophores within the green-red spectral range, while it potentially reduces T state populations in fluorophores emitting in the blue spectral range [13], [14]. Unlike the spectral rule, a systematic addition of [KI] molecules into bromine-free CFl promotes T state build-up. A possible explanation can be that CFl's negative charge reduces the likelihood of close collisional interactions with I^-, thereby making triplet state deactivation via charge transfer less effective in comparison with zwitterionic or positively charged fluorophores such as rhodamine-green (RhGr) [14]. However, [KI] lowers the T state populations of brominated CFls. This outcome is anticipated, as the observed triplet state populations are directly influenced by the ratio of k_{isc}/k_T. As clearly seen from Table II, for the bromine containing CFls, unlike CFl, the relative increment in k_{isc} is smaller than that of k_T, leading to a decrease in the k_{isc}/k_T ratio as [KI] concentration increases.

Next, electronic transitions to longer-lived $\dot{R}^+$ state were investigated separately for each studied dye using proposed microfluidics-based fluorescence microscopy approach. Dark $\dot{R}^+$ state populations were simulated at a slower flow rate of 10 μL/min under same excitation irradiance since these

transitions usually occur in a few milliseconds. $\dot{R}^+$ state populations simulated at different [KI] concentrations were presented in Fig. 4. It is clearly seen that the addition of [KI] externally into each fluorophore solution significantly lowers $\dot{R}^+$ state populations. Although a small anomaly is observed for CFl-4Br in the absence of [KI] (also seen in TRAST experiments [14]), this reduction in $\dot{R}^+$ becomes more pronounced when the degree of bromination is higher. Since [KI] acts as an antioxidant, it helps recover photo-oxidized fluorophores, which leads to a reduction in the population of $\dot{R}^+$ state. As a consequence, fewer fluorophores are likely to remain in the photo-oxidized $\dot{R}^+$ state, and the overall fluorescence can thus be enhanced.

After a rigorous examination of the effects of heavy I^- ions on T and $\dot{R}^+$ state populations, we additionally analyzed how these dark transient states and heavy ions can alter the fluorescence emission of the studied dyes. For this purpose, the peak values of emissive S_1 state populations, e.g. the maximum value in a region where laser beam is positioned, were determined from S_1 signals simulated for each molecule. Max. S_1 populations were computed at varying [KI] concentrations under the same flow rates, that are 10 μL/min and 2000 μL/min, and computed values were plotted in Fig. 5. Computational results indicate that the fluorescence emission of the CFl molecule decreases with increasing [KI] concentration at both flow rates, primarily due to an increase in the population of the T state. On the contrary, incorporation of [KI] into solvent of bromine containing dyes directly promotes S_1 state population owing to a reduction in non-luminescent T and $\dot{R}^+$ states. For this reason, the fluorescence emission becomes much stronger for bromine-containing CFls in the presence of heavy I^- ions. Taken together, the simulation results suggest that the external heavy atom effects can be resolved through employing the microfluidic-based fluorescence microscopy system proposed in this study.

IV. Conclusion

This study demonstrates how non-fluorescent, dark states of CFl-based emitters can be effectively resolved in the presence of heavy I^- ions by using numerical calculations adapted to microfluidics-based fluorescence microscope. By leveraging numerical simulations of fluorescence signals under varying flow rates, we successfully monitored the systematic changes in T and $\dot{R}^+$ state populations at varying [KI] concentrations. While signal broadening, shifts, and decays showed up in $< F_{\text{norm}} >$ signals highlight the impact of internal heavy atom effects, opposite trends were seen due to external heavy atom effects of I^- ions. This enables precise control over fluorophore blinking dynamics through the introduction of heavy ions into solution. Unlike conventional fluorescence techniques, which are often constrained by photobleaching and fluorescence saturation, our approach allows for continuous, high-precision monitoring of long-lived, non-fluorescent states. Beyond fundamental photophysics, this technique holds significant promise for biomedical applications, including macromolecular dynamics, cellular environment studies, and disease diagnostics. Future work can extend this approach to other fluorophores and investigate its potential for detecting subtle biochemical changes in live-cell imaging and drug screening. By integrating fluorescence-based imaging with microfluidics, presented method paves the way for scalable, high-sensitivity detection strategies that could advance both research and clinical applications.

Acknowledgment

Photophysical parameters and electronic transition rates tabulated in Table II were collected from ref. [14] and raw data acquired by performing TRAST measurements can be found from 10.5281/zenodo.7928613. The authors gratefully acknowledge financial support (a project number 124F110) provided by The Scientific and Technological Research Council of Türkiye (TÜBİTAK).

References

[1] C. M. Marian, "Spin-orbit coupling in molecules", *Rev. Comput. Chem.*, vol. 17, pp. 99–204, 2001.

[2] J. R. Lakowicz, *"Principles of Fluorescence Spectroscopy"*, 3rd ed. Boston, MA: Springer, 2006.

[3] J. C. Koziar and D. O. Cowan, "Photochemical heavy-atom effects", *Acc. Chem. Res.*, vol. 11, no. 9, pp. 334–341, 1978.

[4] C. Chen, X. Ni, H. W. Tian, Q. Liu, D. S. Guo, and D. Ding, "Calixarene-based supramolecular AIE dots with highly inhibited nonradiative decay and intersystem crossing for ultrasensitive fluorescence image-guided cancer surgery", *Angew. Chem.*, vol. 132, no. 25, pp. 10094–10098, 2020.

[5] J. Wen, Y. Xu, H. Li, A. Lu, and S. Sun, "Recent applications of carbon nanomaterials in fluorescence biosensing and bioimaging", *Chem. Commun.*, vol. 51, no. 57, pp. 11346–11358, 2015.

[6] H. Lin, Z. Lin, K. Zheng, C. Wang, L. Lin, J. Chen, and J. Song, "Near-infrared-II nanomaterials for fluorescence imaging and photodynamic therapy", *Adv. Opt. Mater.*, vol. 9, no. 9, Art. no. 2002177, 2021.

[7] G. Donnert, C. Eggeling, and S. W. Hell, "Major signal increase in fluorescence microscopy through dark-state relaxation", *Nat. Methods*, vol. 4, no. 1, pp. 81–86, 2007.

[8] S. C. Dirican, B. Tezcan, S. Y. Dölek, and B. Demirbay, "Mikroakışkan temelli floresans mikroskop sistemi ile otofloresan flavin koenzimlerinin fotofiziksel geçişleri üzerine nümerik modelleme çalışmaları", *Int. J. Adv. Eng. Pure Sci.*, vol. 37, no. 1, pp. 73–91, 2025. Available: https://doi.org/10.7240/jeps.1558538

[9] E. Sandberg, B. Demirbay, A. Kulkarni, H. Liu, J. Piguet, and J. Widengren, "Fluorescence bar-coding and flowmetry based on dark state transitions in fluorescence emitters", *J. Phys. Chem. B*, vol. 128, no. 1, pp. 125–136, 2023.

[10] D. L. Shealy and J. A. Hoffnagle, "Beam shaping profiles and propagation", in *Proc. SPIE Laser Beam Shaping VI*, vol. 5876, pp. 99–109, Aug. 2005.

[11] H. T. Beier and B. L. Ibey, "Experimental comparison of the high speed imaging performance of an EM-CCD and sCMOS camera in a dynamic live-cell imaging test case", *PLoS ONE*, vol. 9, no. 1, Art. no. e84614, 2014.

[12] R. Vidunas, "Expressions for values of the gamma function", *Kyushu J. Math.*, vol. 59, no. 2, pp. 267–283, 2005.

[13] A. Chmyrov, T. Sanden, and J. Widengren, "Iodide as a fluorescence quencher and promoter mechanisms and possible implications", *J. Phys. Chem. B*, vol. 114, no. 34, pp. 11282–11291, 2010.

[14] B. Demirbay, G. Baryshnikov, M. Haraldsson, J. Piguet, H. Ågren, and J. Widengren, "Photo-physical characterization of high triplet yield brominated fluoresceins by transient state (TRAST) spectroscopy", *Methods Appl. Fluoresc.*, vol. 11, no. 4, Art. no. 045011, 2023.

[15] S. C. Dirican and B. Demirbay, "A novel microfluidic-based fluorescence detection method reveals heavy atom effects on photophysics of fluorophores with high triplet quantum yield: A numerical simulation study", *Luminescence*, vol. 40, no. 1, Art. no. e70090, 2025.